ADVANCED OPTICAL MATERIALS
www.advopticalmat.de

Materials Views
www.MaterialsViews.com

Directly Metering Light Absorption and Heat Transfer in Single Nanowires Using Metal–Insulator Transition in VO_2

*Chun Cheng, Deyi Fu, Kai Liu, Hua Guo, Shuigang Xu, Sang-Gil Ryu, Otto Ho, Jian Zhou, Wen Fan, Wei Bao, Miquel Salmeron, Ning Wang, Costas P. Grigoropoulos, and Junqiao Wu**

Absorption and propagation of light at the subwavelength length scale is the key process for many technologies such as light management in modern photovoltaics. Similarly, heat exchange and transfer at length scales shorter than the phonon mean free path is critically important for nanoscale thermal management. For such near-field energy conversion and transfer, gauging the energy flow has been either indirect or requires complicated tools.[1,2] Here, we demonstrate a multifunctional powermeter that directly quantifies light absorption and heat transfer at the near-field length scales, such as in a single nanowire. The mechanism is based on the metal–insulator transition (MIT) in single-crystal vanadium dioxide (VO_2) microbeams,[3] where the domain wall moves free of kinetic obstruction and exhibits distinct optical contrast between the two phases. The powermeter is contactless and optically readable, allowing quick determination of local temperature, optical absorbance, thermal conductivity, and contact thermal resistance of single nanostructures.

The MIT of VO_2 occurs at T_C = 68 °C between an insulating (I), optically reflective phase at lower temperatures and a metallic (M), optically absorptive phase at higher temperatures.[4,5] The phase transition is first order, and is highly sensitive to doping,[6,7] stoichiometry,[8] and local strain.[3,9] In contrast to the diffusive and percolative transition in substrate-clamped, polycrystalline VO_2 thin films,[10,11] strain-free, single-crystalline VO_2 nanobeams support an intrinsically abrupt MIT, where the M/I domain wall moves freely along the nanobeam axis in response to local temperature variation, akin to a 1D frictionless waveguide.[3,9,12] This effect works as the basic mechanism of the near-field powermeter (NFP), as shown in **Figure 1**a,b. Here the term "near-field" is used to emphasize the fact that the size of studied objects is comparable to the characteristic length in question, such as light wavelength or phonon mean free path.

In Figure 1a,b, a single-crystalline VO_2 nanobeam (or microbeam) with a uniform rectangular cross-section (Figure S1, Supporting Information) is cantilevered from a silicon substrate, where the root is clamped by Pt deposited with a focused ion beam (FIB) to ensure a good thermal sink.[13,14] A continuous-wave laser is focused at a targeted position along the nanobeam providing local heating. The device is placed in vacuum ($\lesssim 1 \times 10^{-3}$ Torr) and operates at relatively low temperature ($\lesssim$150 °C); therefore, the heat loss to air and thermal radiation are several orders of magnitude smaller than the heat dissipation to the substrate, as we have evaluated in a previous work.[15] When the laser intensity exceeds a threshold, the tip-side portion of the VO_2 beam is heated to temperatures above T_C, such that an M/I domain wall appears along the VO_2 beam between the laser spot and the root. Due to the nature of the phase transition, there is a hysteresis or superheating/cooling effect when the M/I domain wall is created/eliminated by tuning the laser power above/below the power threshold. However, different from the case in Andrew et al.,[16] our VO_2 beams are clamped on one end only, thus is freestanding and free of strain accumulation. Therefore, the axial strain-induced wide hysteresis is absent here. After creation of the M/I domain wall, the domain wall moves relatively freely along the nanobeam as if it is a "wall waveguide". Moreover, the extremely clean and smooth surface facet of the VO_2 beams used (see Figure S1, Supporting Information) minimizes domain wall pinning effects.[17] Indeed, the fact that the domain wall position scales nearly perfectly with the laser power in Figure 1c,d indicates the free motion of the domain wall without pinning and kinetic obstruction. Despite this, there may indeed exist a small hysteresis of ≈2 °C in the MIT as measured in our previous work.[6] Therefore, we add corresponding error bars for the data plotted in the following to represent the uncertainty of temperature at the domain wall.

The M/I domain wall indicates the location where the local temperature is T_C with ≈2 °C uncertainty; hence, the single VO_2 beam acts as a nanoscale thermometer that can be optically read out. Considering the 1D thermal conduction along the

Prof. C. Cheng, Dr. D. Fu, Dr. K. Liu, O. Ho, Dr. J. Zhou, Dr. W. Fan, W. Bao, Prof. M. Salmeron, Prof. J. Wu
Department of Materials Science and Engineering
University of California
Berkeley, CA 94720, USA
E-mail: wuj@berkeley.edu

Prof. C. Cheng
Department of Materials Science and Engineering
South University of Science and Technology
Shenzhen, Guangdong 518055, China

Prof. C. Cheng, Dr. K. Liu, Dr. H. Guo, W. Bao, Prof. M. Salmeron, Prof. J. Wu
Materials Sciences Division
Lawrence Berkeley National Laboratory
Berkeley, CA 94720, USA

Prof. C. Cheng, Dr. S.-G. Ryu, Prof. C. P. Grigoropoulos
Department of Mechanical Engineering
University of California
Berkeley, CA 94720, USA

Dr. S. Xu, Prof. N. Wang
Department of Physics
Hong Kong University of Science and Technology
Hong Kong, China

DOI: 10.1002/adom.201400483

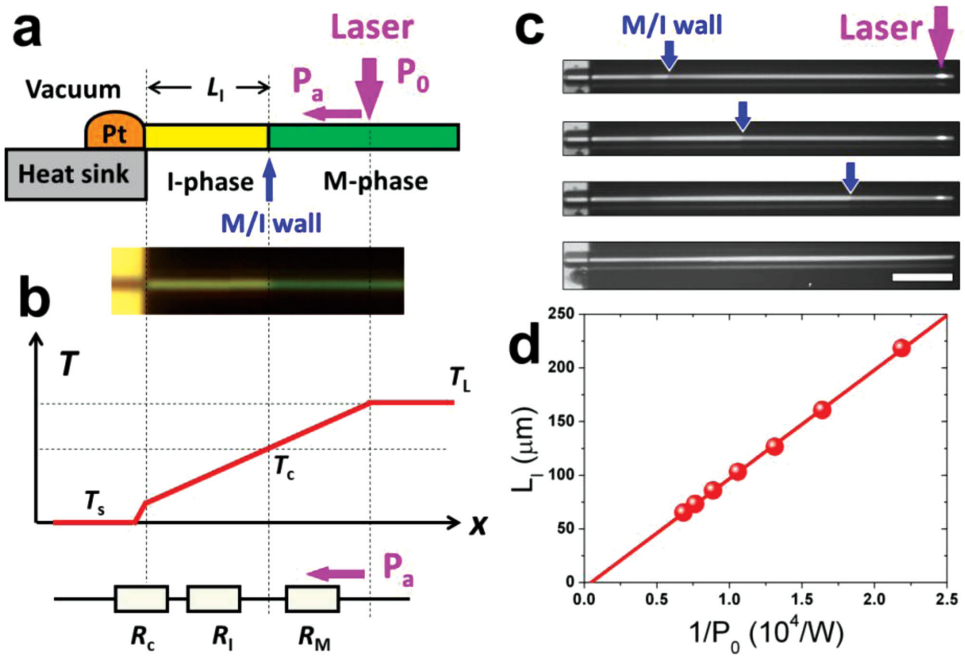

Figure 1. Working principle of the near-field powermeter (NFP). a) A focused laser beam thermally activates a metal domain in a cantilevered VO_2 micro/nanobeam. The optically read M/I domain wall indicates the position where the temperature is the MIT temperature T_C. b) Schematic of temperature profile along the VO_2 microbeam. Between (a) and (b) is a color optical image of a heated VO_2 nanobeam. c) The M/I wall moving toward the root of a VO_2 microbeam with increasing (bottom to top) laser power. The laser polarization is parallel to the microbeam axis. Scale bar is 50 μm. d) Length of the I domain is inversely proportional to the incident laser power. The slope and interception with the vertical axis give optical absorbance (α) and contact thermal resistance (R_C) of the VO_2 microbeam, respectively.

VO_2 beam with crosssection area A, the absorbed optical power flow (P_a) is given by:

$$P_a = \frac{\Delta T}{R_c + L_I/(\kappa_{VO_2} A)} \quad (1)$$

where ΔT = 46 °C, the temperature difference between the domain wall (T_C) and substrate (T_S), κ_{VO_2} is the thermal conductivity of VO_2, taken to be 6.5 W m^{-1} K^{-1} for both the M and I phases in this work (see Supporting Information for details),[5,15] L_I is the I-domain length, and R_C is the contact thermal resistance at the Pt bond. The optical absorbance of the VO_2 nanobeam is defined as $\alpha \equiv P_a/(\beta P_0)$, where P_0 is the total incident laser power that is measured with a commercial powermeter placed directly below the nanobeam. The geometrical factor β is the percentage of the incident laser power physically striking the nanobeam, which is calculated by integrating the incident Gaussian laser beam energy over the area of nanobeam exposed to the laser (see Supporting Information). From Equation (1), it can be seen that L_I is linearly proportional to $1/P_0$. The interception of this dependence with the L_I axis gives the contact thermal resistance R_C, and the slope gives the absorbance α. As shown in Figure 1c, L_I is progressively shorter with stronger P_0. The data are plotted in Figure 1d from which R_C and α are determined to be 1.2×10^5 K W^{-1} and 0.74, respectively, for the VO_2 nanobeam.

We note that the measured α is found to be independent of the laser focus position (see Supporting Information). This justifies the assumption that heat dissipation to the ambient (including heat loss to air and thermal radiation) is indeed negligible, in agreement with previous work.[15] In addition, we found that R_C must be taken into account for accurate evaluation of α, although it is less than 10% of the typical nanobeam thermal resistance (of the order of 10^6–10^7 K W^{-1}, see Supporting Information). R_C has been difficult to quantify in nanoscale systems, whereas here it is directly determined independently from other parameters.

After demonstration of quantifying optical absorbance of single VO_2 nanobeams, next we extend the application of VO_2 NFP to measuring optical absorption of other nanomaterials. Here we take Si nanowires as an example. In **Figure 2**a, a Si nanowire is Pt-bonded to the tip of the VO_2 NFP. The laser beam is focused on the Si nanowire to activate the MIT of the NFP, resulting in a clearly resolved M/I domain wall as shown at the bottom in Figure 2a. As energy is injected at the laser spot on the Si nanowire, it entirely flows unidirectionally toward the substrate; therefore, the Si thermal conductivity (κ_{Si}) and junction thermal resistance between Si and VO_2 (R_{CJ}) are not needed for the calculation. As a result, P_a of the Si nanowire can be obtained using the same procedure as shown in Figure 1 and Equation (1). Figure 2b shows P_a of four Si nanowires with different radii. The slope of the P_a–P_0 dependence increases with the nanowire radius, which is mostly attributed to the larger β factor for larger radius nanowires. Tens of Si nanowires with a wide range of radii were measured, and the measured α is plotted in Figure 2c. To minimize errors, these Si nanowires were grouped into a few groups, where each group corresponds to nanowires bonded to and

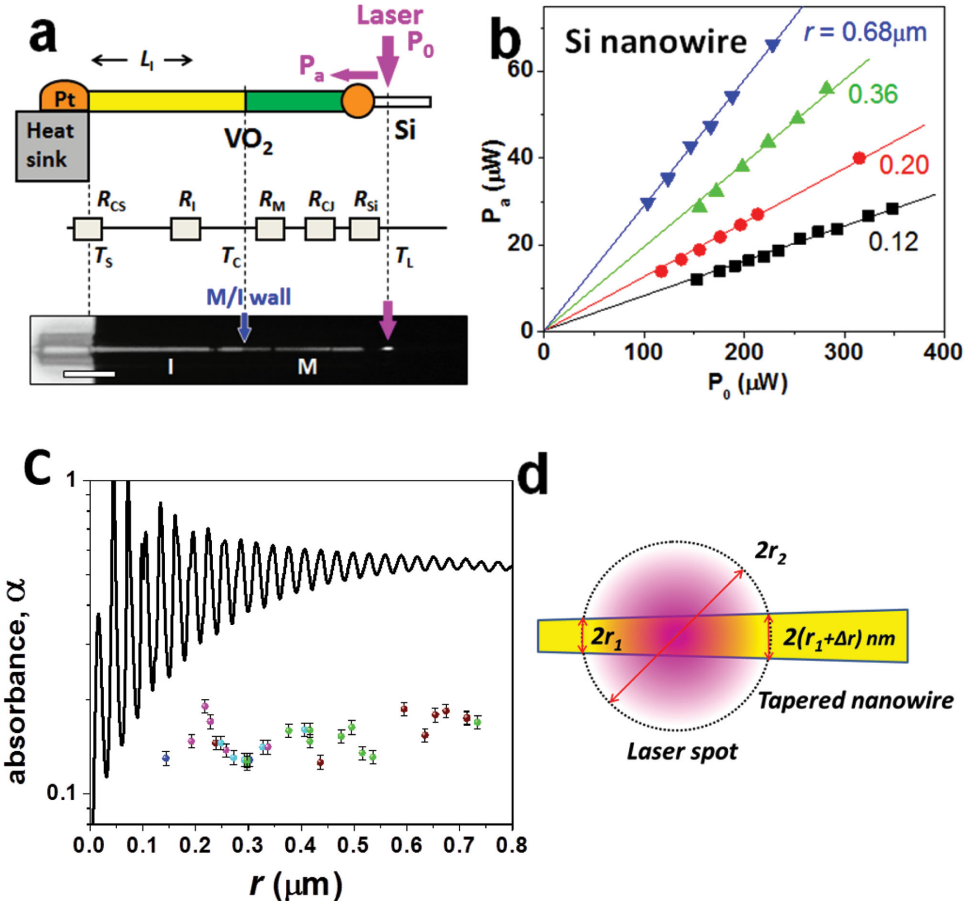

Figure 2. Quantifying optical absorbance of a single Si nanowire. a) The NFP is bonded to a Si nanowire, allowing quantification of optical absorption of the single Si nanowire. Scale bar is 20 μm. b) Absorbed power of four Si nanowires with different radii. c) The optical absorbance (α) of Si nanowires with a wide range of radius r. Each color of data points corresponds to a series of Si nanowires bonded to the same VO_2 nanobeam as an NFP. Also shown are the analytical calculated results. The error bars in panel c show the approximate range of error for all the data points, and primarily originate from uncertainties in measuring the M domain lengths, P_0, and the T_C hysteresis (≈2 °C). d) Schematic of a tapered Si nanowire under illumination of a focused Gaussian laser beam.

measured using the same VO_2 nanobeam NFP (see Figure S4 in Supporting Information).

The results in Figure 2c show that the optical absorbance of individual Si nanowire distributes from 0.1 to 0.2. For comparison, also shown in Figure 2c is the analytically calculated α of smooth Si nanowires. It can be seen that the calculated α exhibits strong oscillations as a function of nanowire diameter due to optical interference, which has been theoretically predicted by several groups,[18–20] yet no experimental data on single nanowire absorption have been reported. Our measured α shows a much weaker oscillation and relatively low values. We attribute the lack of expected oscillations in the measured α to the tapered morphology of the studied nanowires. The Si nanowires used in our experiments were grown with the established Au-catalyzed VLS growth method. TEM imaging has shown high crystalline quality and smooth surface of these nanowires (see images in Figure S2, Supporting Information). However, the as-grown Si nanowires were inevitably tapered because of the gradual volume shrinkage of Au catalyst nanoparticles during the nanowire growth. As reported by Brittman et al.,[19] if the nanowire diameter changes by only 20 nm over 9.5 μm, the tapering would significantly broaden the nanowire optical resonances. Doerk et al.[20] also point out that the tapered morphology of Si nanowires may be responsible for the discrepancy between the calculated absorption and actual values. As to our case, the radius of the tapered nanowires changes about 10 nm μm^{-1}. According to the analytical calculation (see Figure 2c) on absorption as a function of nanowire radius, a variation of radius of ≈14 nm will displace the oscillation peak to the neighboring oscillation valley. Therefore, within the laser spot size (≈1.3 μm) on the nanowire, the effective nanowire radius varies by ≈13 nm. So the signal is effectively a convolution of signals from nanowires with radius varying by this much, which would smear out the oscillation.

Furthermore, the measured α values are systematically lower compared to the theoretical predictions. We attribute this discrepancy to possible underestimation of the laser beam spot size. Typically, the laser beam size is calculated by $2r_2 = \frac{2\lambda}{\pi \times N_A}$, where r_2 is the laser beam radius, λ is the wavelength of laser, and N_A is the numerical aperture of the used objective lens. However, the actual laser beam size could be significantly

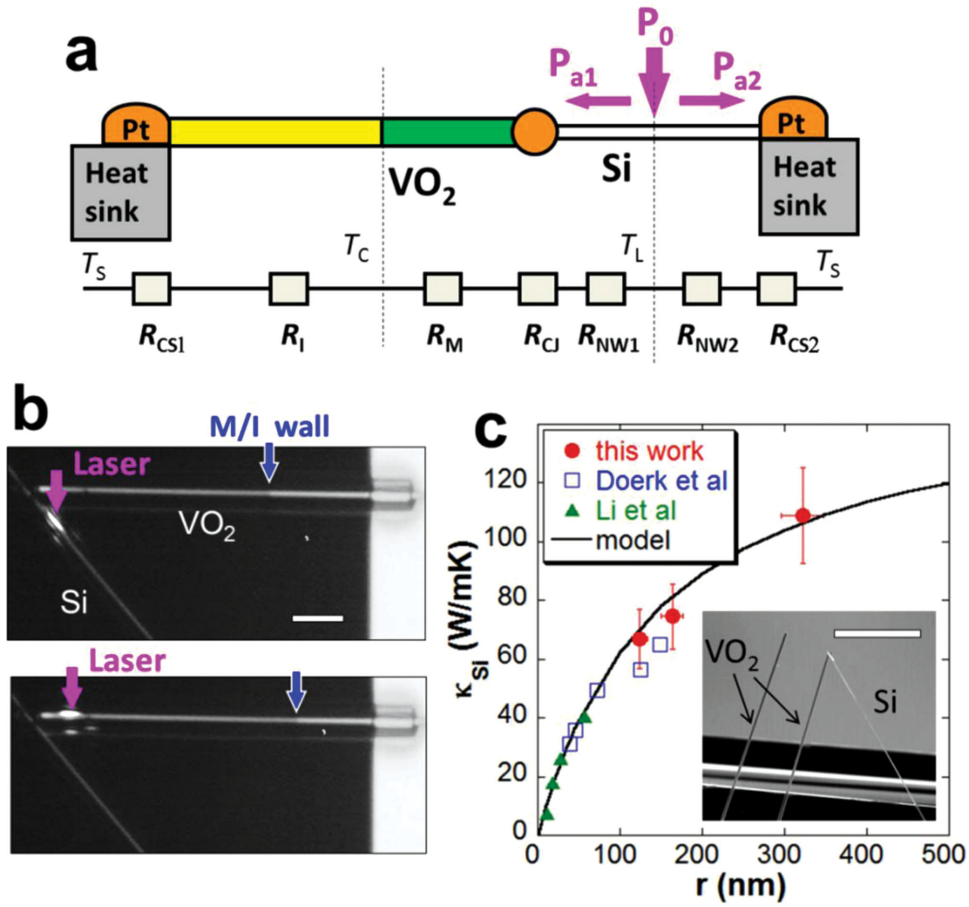

Figure 3. Measuring thermal conductivity (κ) of a single nanowire with the NFP. a) A Si nanowire is bonded to a VO_2 NFP, and the other ends of both Si and VO_2 are clamped to heat sink. A laser beam inputs energy onto the VO_2 or the Si nanowire; the M/I wall position along the VO_2 is measured, from which κ_{Si} of the Si nanowire is extracted. b) Optical image of a bonded VO_2–Si nanowire system, where M/I wall position depends on the laser intensity and focus position. Scale bar is 20 μm. c) Measured room-temperature thermal conductivity of three Si wires with different radii. Inset shows the overview of the device used. Scale bar is 100 μm. In addition to the bonded VO_2–Si nanowire system, another identical VO_2 microbeam is used to determine the optical absorbance of VO_2 which is needed for calibration of the NFP. To ensure uniform optical and thermal properties, both VO_2 segments were cut from a single, long VO_2 microbeam with uniform crosssection. The error bars show the approximate range of error for all the data points, and primarily originate from uncertainties in measuring the M domain lengths, the nanowire radius, P_0, laser focus, and the T_C hysteresis.

larger than the calculated one, because a small off-focus of the laser may result in a larger illumination area, which leads to a larger β and then a smaller optical absorbance for $\alpha \equiv P_a/(\beta P_0)$. However, we recognize that the actual laser spot size is difficult to determine by experiments. Therefore, for comparison and as an upper bound, we provide a new set of α in Figure S9 in the Supporting Information assuming that the laser spot radius is 200% larger.

We note that because of difficulty in directly measuring the energy flow in nanowires, the optical absorption of individual nanowires has been routinely evaluated using these analytical equations for α on applications ranging from Raman thermography to photonics and photovoltaics.[1,20,22] However, our work shows deviations between the real nanowire absorption and theoretical prediction.[1,18–20] These call for caution in using these equations or simulation results. Despite the uncertainty in determination of the actual laser beam spot size, our work provides a way for quantitative evaluation of optical absorbance in individual nanowire by gauging energy flow using the NFPs. This is similar in spirit to the electron-beam heating microthermometers using the VO_2 nanobeams as we and co-workers recently demonstrated.[23]

Furthermore, we show another independent function of the NFP where it is used to evaluate thermal conductivity of a single nanowire. Accurate determination of the thermal conductivity of individual nanowires has always been challenging, which typically involves multilevel microfabrication and photo/electron-beam lithography,[2,24] or high-sensitivity Raman thermography which has limited accuracy because α of single nanowires is needed.[20] In our NFP approach, the device is composed of a cantilevered VO_2 NFP bonded with the nanowire to be measured (again using Si nanowire as an example), where the other ends of the nanowires are bonded to the substrate, as shown in **Figure 3**a,b. The laser beam injects energy onto the Si nanowire or the VO_2 nanobeam, and the M/I domain wall positions along the VO_2 nanobeam are used to determine the Si nanowire thermal conductivity (κ_{Si}), which is given by a combination of the laser position, the M/I domain wall position, the

thermal conductivity of VO_2 (κ_{VO2}), and the optical absorbance α_{Si} and α_{VO2} (see Supporting Information). It is noted that the contact resistance between the wire and the substrate (R_{CS1} and R_{CS2}) can be safely ignored because they are less than 10% of the thermal resistance of the typical sample (VO_2 and Si wires). This treatment is the same as that used in previous work.[25,26] In addition, the junction contact resistance (R_{CJ}) is nicely cancelled out from the final expression from the calculation of κ_{Si} (see Supporting Information for details). The measured κ_{Si} values of three Si wires with different diameters are shown in Figure 3c. For comparison, we have also included Si nanowire thermal conductivity previously measured using microfabricated suspended pads and by Raman thermography.[20,25] Also included for comparison is the Si nanowire thermal conductivity model calculated by assuming that the only additional phonon scattering is the fully diffusive surface scattering. A reasonable agreement is seen between these data and the calculation.

In summary, a multifunctional NFP is developed based on the MIT in VO_2. The optically resolved metal–insulator domain wall moving along the VO_2 nanobeam enables direct, quantitative determination of local temperature, absorbed light power, and thermal conductivity of individual nanowires. In case of geometrically and/or compositionally complicated nanostructures, simulation or other means of evaluating light absorption becomes significantly more challenging, but the VO_2-based NFP is still easily applicable. As the MIT temperature of VO_2 can be tuned to other temperatures by doping,[6,7] the operation temperature range of the NFP can be expanded beyond near room temperature. Combined with spatial temporally resolved techniques such as laser pumping and probing, it is possible to extend this tool to the time domain for direct quantification of dynamics of energy-carrying charges and phonons in individual nanostructures.

Experimental Section

Sample and Device Preparation: The VO_2 beams were synthesized using the vapor transport method developed recently.[14] V_2O_5 powder was placed in a quartz boat in the center of a horizontal tube furnace. The reaction product was collected on substrates downstream from the source quartz boat. The growth was carried out in the following condition: evaporation temperature ≈880 °C, Ar carrier gas flow rate ≈6.8 sccm, pressure ≈5 Torr, and evaporation time ≈2 h or more. Ultralong, high-dense, freestanding, single-crystal VO_2 micro/nanobeams were collected on rough (unpolished) surface of quartz substrates. Si nanowires were fabricated on a Si wafer with gold nanoparticles as the catalysts.[21] The Si vapor source was silane gas (purity >99.99% and flow rate 15 sccm) which was mixed with hydrogen (purity >99.99% and flow rate of 100 sccm) and fed into the reaction quartz tube (pressure was about 50 Torr) placed in a furnace. High-quality Si nanowires grew at about 520 °C

Freestanding VO_2 micro/nanobeams were transferred onto Si substrates and cut into segments with lengths of 100–300 μm using microprobe tips on a CASCADE M150 probe station. Then the VO_2 beams were cantilevered to the edge of the Si substrate. The Si micro/nanowires to be measured were transferred and coupled to the VO_2 nanobeams by microprobes. To reduce contact thermal resistance, Pt pads were deposited at the roots and junctions of wires using Ga^+ beam (30 kV) induced deposition inside a FEI-Quanta 3D Dual Beam FIB. The coupled VO_2–Si devices were loaded into a vacuum chamber for further investigation.

Measurements: For the optical absorbance and thermal conductivity measurements of single micro/nanowires with different radii, we carried out experiments on the home-made laser thermography setup (see Figure S3 in the Supporting Information). The vacuum chamber was pumped down to $<10^{-3}$ Torr by a mechanical pump. Optical images of devices were recorded using an optical microscope equipped with a CCD camera. The laser heating of cantilevered devices was carried out using the microscope with continuous-wave Ar ion laser (wavelength 514.5 nm). The stage can be moved in the *x*–*y* plane with respect to the laser spot, and the laser power is tuned by an assembly of beam splitter and neutral filters. The size of the focused laser spot is less than 2 μm. The maximum safe laser power was determined by causing permanently visible damage on the surface of a VO_2 or Si nanowire with the focused laser, and much lower laser intensities were used in subsequent experiments. For each measurement, the laser focal depth and position with respect to the nanowire were carefully adjusted until a maximum M domain length is reached at the VO_2 NFP, so as to eliminate misalignment. The laser polarization direction was kept always parallel to the axis direction of the studied nanowire to eliminate influence from the polarization effect. The total incident laser power P_0 was measured with a commercial powermeter (Thorlabs, S120C).

Supporting Information

Supporting Information is available from the Wiley Online Library or from the author.

Acknowledgements

The authors thank Prof. Jie Yao for helpful discussions. This work was supported by the National Science Foundation (NSF) under Grant No. ECCS-1101779. C. C. is partially supported by National Natural Science Foundation of China (Grant No. 51406075), startup grants from the South University of Science and Technology of China, and the Hong Kong Research Grants Council through RGC projects (FSGRF14SC31 and WMINST11SC04).

Received: October 22, 2014
Published online: January 2, 2015

[1] L. Cao, J. S. White, J. Park, J. A. Schuller, B. M. Clemens, M. L. Brongersma, *Nat. Mater.* **2009**, *8*, 643.
[2] P. Kim, L. Shi, A. Majumdar, P. McEuen, *Phys. Rev. Lett.* **2001**, *87*, 215502.
[3] J. Wu, Q. Gu, B. S. Guiton, L. Ouyang, N. de Leon, H. Park, *Nano Lett.* **2006**, *6*, 2313.
[4] V. Eyert, *Ann. Phys.* **2002**, *11*, 650.
[5] C. N. Berglund, H. J. Guggenheim, *Phys. Rev.* **1969**, *185*, 1022.
[6] S. Lee, C. Cheng, H. Guo, K. Hippalgaonkar, K. Wang, J. Suh, K. Liu, J. Wu, *J. Am. Chem. Soc.* **2013**, *135*, 4850.
[7] Q. Gu, A. Falk, J. Wu, L. Ouyang, H. Park, *Nano Lett.* **2007**, *7*, 363.
[8] S. Zhang, I. S. Kim, L. J. Lauhon, *Nano Lett.* **2011**, *11*, 1443.
[9] J. Cao, E. Ertekin, V. Srinivasan, W. Fan, S. Huang, H. Zheng, J. W. L. Yim, D. R. Khanal, D. F. Ogletree, J. C. Grossman, J. Wu, *Nat. Nanotechnol.* **2009**, *4*, 732.
[10] M. M. Qazilbash, M. Brehm, B. Chae, P. C. Ho, G. O. Andreev, B. Kim, S. J. Yun, A. V. Balatsky, M. B. Maple, F. Keilmann, H. Kim, D. N. Basov, *Science* **2007**, *318*, 1750.
[11] D. Fu, K. Liu, T. Tao, K. Lo, C. Cheng, B. Liu, R. Zhang, H. Bechtel, J. Wu, *J. Appl. Phys.* **2013**, *113*, 043707.
[12] J. Wei, Z. Wang, W. Chen, D. H. Cobden, *Nat. Nanotechnol.* **2009**, *4*, 420.

[13] B. S. Guiton, Q. Gu, A. L. Prieto, M. S. Gudiksen, H. Park, *J. Am. Chem. Soc.* **2005**, *127*, 498.
[14] C. Cheng, K. Liu, B. Xiang, J. Suh, J. Wu, *Appl. Phys. Lett.* **2011**, *100*, 103111.
[15] C. Cheng, W. Fan, J. Cao, C. P. Grigoropoulos, J. Wu, *ACS Nano* **2011**, *5*, 10102.
[16] J. C. Andrew, B. Samuel, W. Jiang, C. David, R. B. Markus, *Nano Lett.* **2010**, *10*, 1574.
[17] H. Guo, K. Chen, Y. Oh, K. Wang, C. Dejoie, S. A. Syed Asif, O. L. Warren, Z. W. Shan, J. Wu, A. M. Minor, *Nano Lett.* **2011**, *11*, 3207.
[18] F. J. Lopez, J. K. Hyun, U. Givan, I. S. Kim, A. L. Holsteen, L. J. Lauhon, *Nano Lett.* **2012**, *12*, 2266.
[19] S. Brittman, H. Gao, E. C. Garnett, P. Yang, *Nano Lett.* **2011**, *11*, 5189.
[20] G. S. Doerk, C. Carraro, R. Maboudian, *ACS Nano* **2010**, *4*, 4908.
[21] S. Dai, J. Zhao, L. Xie, Y. Cai, N. Wang, J. Zhu, *Nano Lett.* **2012**, *12*, 2379.
[22] J. Giblin, V. Protasenko, M. Kuno, *ACS Nano* **2009**, *3*, 1979.
[23] H. Guo, M. I. Khan, C. Cheng, W. Fan, C. Dames, J. Wu, A. M. Minor, *Nat. Commun.* **2015**, *5*, 4986.
[24] S. Dhara, H. S. Solanki, A. R. Pawan, V. Singh, S. Sengupta, B. A. Chalke, A. Dhar, M. Gokhale, A. Bhattacharya, M. M. Deshmukh, *Phys. Rev. B* **2011**, *84*, 121307.
[25] D. Li, Y. Wu, P. Kim, L. Shi, P. Yang, A. Majumdar, *Appl. Phys. Lett.* **2003**, *83*, 2934.
[26] L. Shi, D. LI, C. Yu, W. Jang, D. Kim, Z. Yao, P. Kim, A. Majumdar, *J. Heat Transfer* **2003**, *125*, 881.